Organic & Biomolecular Chemistry

PAPER

View Article Online
View Journal | View Issue

Cite this: *Org. Biomol. Chem.*, 2018, **16**, 2499

Designing phenylalanine-based hybrid biological materials: controlling morphology *via* molecular composition†

Srinivas Mushnoori,[a] Kassandra Schmidt,[b] Vikas Nanda[c,d] and Meenakshi Dutt*[a]

Received 16th January 2018,
Accepted 10th March 2018

DOI: 10.1039/c8ob00130h

rsc.li/obc

Harnessing the self-assembly of peptide sequences has demonstrated great promise in the domain of creating high precision shape-tunable biomaterials. The unique properties of peptides allow for a building block approach to material design. In this study, self-assembly of mixed systems encompassing two peptide sequences with identical hydrophobic regions and distinct polar segments is investigated. The two peptide sequences are diphenylalanine and phenylalanine-asparagine-phenylalanine. The study examines the impact of molecular composition (namely, the total peptide concentration and the relative tripeptide concentration) on the morphology of the self-assembled hybrid biological material. We report a rich polymorphism in the assemblies of these peptides and explain the relationship between the peptide sequence, concentration and the morphology of the supramolecular assembly.

Introduction

Recent advances in novel biological materials *via* peptide self-assembly have been driven by their potential use in a wide range of applications, such as neurodegenerative disease treatment,[1–6] therapeutics,[6–11] peptide-based electronics[12–15] and nanobiomaterials.[16–24] Earlier studies have reported peptides to assemble into nanofibers,[25–29] nanotubes,[30–37] vesicles[38–42] and nanosheets.[41,43] Peptides are composed of a combination of any number of 20 amino acids. This allows for a unique building block approach to biological material design, providing a high degree of control over the morphology of supramolecular peptide assemblies.

Among the various peptide sequences employed for creating biological materials, diphenylalanine has been extensively studied using experimental approaches[30,32,37,44–49] and computational techniques.[48,50,51] It is a small and stable peptide that has been reported to form supramolecular assemblies including vesicles and nanotubes.[50–53] More recently, diphenylalanine derivatives such as triphenylalanine (FFF) and diphenylalanine-fluorenylmethyloxycarbonyl chloride (FF-Fmoc) have been explored for their potential to self-assemble into nanostructures. These efforts have found a large diversity of assemblies including nanowires, ribbons and nanofibers.[54] The primary focus of these studies has been in developing nanostructures self-assembled from a single peptide sequence.

The creation of nanostructures with specific control on their material characteristics can be fulfilled by using a variety of peptide sequences. The contribution of each sequence and the synergistic interplay between their molecular characteristics can generate materials with specific sequence–property relationships. An earlier computational study reported mixtures of diphenylalanine and triphenylalanine for generating toroidal structures,[54] which were verified experimentally. Yet, there is a dearth in the understanding of sequence–property relationships of biological materials encompassing distinct peptide sequences. In addition, very little is known about the mechanics of the assembly of distinct peptide sequences to form a hybrid biological material with target properties.

In this study, we examine the impact of molecular composition on the properties (specifically, morphology) of self-assembled hybrid biological materials. For simplicity, we focus on diphenylalanine (FF) and its derivative phenylalanine-asparagine-phenylalanine (FNF). The derivative changes the sequence of diphenylalanine by the addition of asparagine between the two phenylalanine groups. In addition, these two sequences allow us to examine the impact of differences in the

[a]*Department of Chemical and Biochemical Engineering, Robert Wood Johnson Medical School, Rutgers The State University of New Jersey, Piscataway, New Jersey, USA. E-mail: meenakshi.dutt@rutgers.edu*
[b]*Department of Biomedical Engineering, Robert Wood Johnson Medical School, Rutgers The State University of New Jersey, Piscataway, New Jersey, USA*
[c]*Center for Advanced Biotechnology and Medicine, Robert Wood Johnson Medical School, Rutgers The State University of New Jersey, Piscataway, New Jersey, USA*
[d]*Department of Biochemistry and Molecular Biology, Robert Wood Johnson Medical School, Rutgers The State University of New Jersey, Piscataway, New Jersey, USA*
†Electronic supplementary information (ESI) available. See DOI: 10.1039/c8ob00130h

polar groups of the peptide species on the self-assembled hybrid material morphology. We vary the molecular composition through the total concentration of the peptides and the relative concentration of the tripeptide (FNF). We address the large molecular composition parameter space by adopting a computational approach (namely, the molecular dynamics simulation technique), which is used in conjunction with a coarse-grained force field. We find that the total concentration of the peptides along with the relative concentration of the tripeptides can control the morphology of the hybrid assemblies. The results from this study provide insights into (1) assembly mechanics of specific peptide sequences, and (2) shape control of supramolecular nanostructures.

Computational methods

The assembly of diphenylalanine (FF) and phenylalanine-asparagine-phenylalanine (FNF) was promoted by the hydrophobic effect. We used the molecular dynamics (MD) simulation technique to capture the dynamics of the aggregation process along with the structure and morphology of the hybrid peptide materials. This required simulating the aggregation of several hundreds of molecules that were dispersed in an aqueous environment. An all-atom representation of the molecules would have been too demanding in terms of computational resources in resolving the temporal scales associated with the assembly process along with capturing the multiscale structural characteristics of the self-assembled material. To circumvent this difficulty, we employed coarse-grained representations of the peptides.

For this study, we used the Martini v2.2 coarse-grained (CG) force field[55] for biomolecules,[56,57] an established, generalizable force field that has been demonstrated to capture the behavior of a wide range of biomolecules. Atoms of the peptides were mapped using the Martini CG model[57] (see Fig. 1). Particle type P5 was used for the backbone of each residue, as well as for the sidechain of asparagine. Three SC5 particles were used to represent the aromatic sidechain of phenylalanine. Since the peptides are assumed to be in a zwitterionic state, charges of $+1e$ and $-1e$ were assigned to the N and C termini, respectively. The CG mapping details are presented in ESI Tables 1 and 2† and are represented graphically in Fig. 1. van der Waals forces were represented by a 12-6 Lennard-Jones approximation, while electrostatics were calculated using a shifted Coulomb potential. All cutoffs were maintained at 1.2 nm in accordance with the Martini CG model.

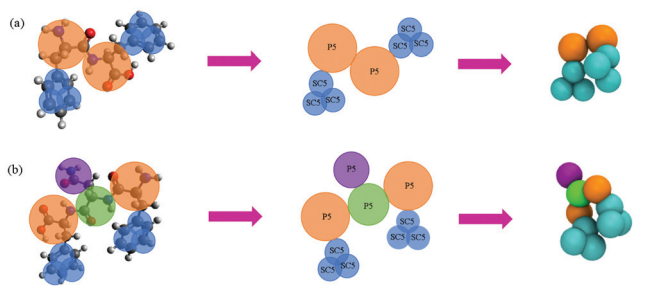

Fig. 1 Coarse-grained mapping details for (a) diphenylalanine (FF) and (b) phenylalanine-asparagine-phenylalanine (FNF). Coarse-grained representations of the peptides in the molecular dynamics simulations shown on the right side.

Simulations were performed using the GROMACS package (v5.2.1).[58–62] The simulations were set up by using the inbuilt GROMACS functions to insert the FF and FNF molecules into the simulation box and solvate them. Since the system is charge neutral, no counterions are required. To prevent physically unrealistic freezing of the Martini water,[55] a 0.1 mole fraction of antifreeze particles was maintained. The system was then energy minimized by using a steepest descent integrator to remove any overlaps between the particles. This was followed with a 500 ps (effective time) equilibration followed by a production simulation for 4 μs (effective time). The duration of the production simulation was selected so as to generate a single, stable self-assembled nanostructure.

All simulations were carried out in the isothermal-isobaric ensemble. The temperature was maintained at 310 K (ref. 50, 54) using velocity rescaling with a stochastic term to ensure correct sampling.[63,64] Pressure was maintained at 1 bar using a Parrinello–Rahman barostat.[65–67] The timestep was maintained at 25 fs and all simulations were run for an effective time of 4 μs. The neighbor lists were updated every 0.25 ps with a 1.2 nm cutoff. The particle trajectories were sampled every 0.25 ns for analysis and visualization. The LINCS algorithm was employed to constrain bond lengths in the aromatic phenylalanine sidechains.

All the simulations were carried out using systems encompassing a total of 500 peptide molecules. The peptide molecules were assumed to exist in a zwitterionic state. The total peptide concentration was controlled by pre-selecting the box size and appropriately populating the box with solvent beads. The relative tripeptide concentrations were implemented by varying the ratio of dipeptides (FF) to tripeptides (FNF), while still maintaining the total number of peptide molecules to 500.

We examined 5 total peptide concentrations (0.1, 0.15, 0.2, 0.25 and 0.3 peptides per nm^3) and 11 relative tripeptide concentrations (ranging from 0% to 100%). The results for each system were based upon 10 independent particle trajectories. Hence, the study is based upon a total of 550 simulations. Further details of the simulation box are provided in ESI Table 3.†

While interpreting timescales in simulations that use the Martini coarse-graining scheme, a four-fold speedup is assumed in the diffusion dynamics as compared to real systems, since the Martini force field's reduced frictional component from the removal of atomistic degrees of freedom leads to a smoother energy landscape.[55] Therefore, unless explicitly stated, we use an "effective" time instead of the simulation time for the remainder of this paper.

Results and discussion

All molecular compositions explored in this study are observed to spontaneously assemble into nanostructures encompassing bilayers. The assembly is driven by the hydrophobic effect, wherein the hydrophobic aromatic rings of the phenylalanine side chains minimize their interface with the solvent by preferentially interacting with other aromatic sidechains. In addition, the hydrophilic backbones and asparagine side chains preferentially interact with the solvent particles. These simultaneous processes drive peptide aggregation, which continues until a single, stable aggregate forms for the duration of the simulation.[50,54,68–72]

The morphology of the hybrid nanostructures can be classified into three categories based on their relationship in the three spatial dimensions. We classify a structure as "open" in a given spatial direction if one of the following criteria is met: (i) it extends infinitely (through periodic walls) along that direction, or (ii) if it does not extend infinitely in a given direction, two edges of the bilayer perpendicular to that direction are exposed to the solvent. Therefore, if the bilayer of the nanostructure is open in two dimensions, it is classified as a lamella, it may extend infinitely along two axes, or along one axis but has edges exposed to the solvent. If the bilayer of the nanostructure is closed in all three spatial dimensions (*i.e.* does not extend infinitely through periodic walls), it is classified as a vesicle. In the event that the bilayer of the nanostructure is closed in two dimensions but extends infinitely in the third dimension, it is classified as a nanotube. Representatives of these assemblies are shown in Fig. 2a–c. The cross-sectional views of the vesicle (see Fig. 2a) and the nanotube (see Fig. 2b) indicate the presence of an internal cavity in the nanostructures. The internal cavity is stabilized by the interface between the solvent and the hydrophilic backbones and asparagine side chains.

There is a fourth category of self-assembled nanostructures, which is not representative of an organized morphology. These nanostructures are classified as "disordered" assemblies. Although the peptide species in these nanostructures are organized into bilayers at a local scale, their morphology cannot be classified as vesicles, nanotubes or lamellae. The morphologies of the nanostructures for different molecular compositions are summarized in Table 1.

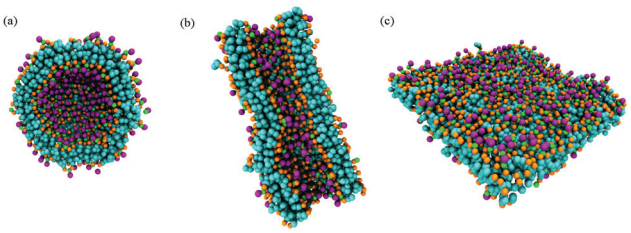

Fig. 2 Self-assembled hybrid nanostructures: (a) diametrical cross-sectional view of a vesicle, (b) cylindrical axis cross-sectional view of a nanotube, and (c) lamellar bilayer.

Table 1 Summary of the morphologies for the hybrid nanostructures for different values of the total and relative concentration of the peptide molecules

Total peptide conc. (peptides per nm^3)	0% Tripeptide			10% Tripeptide			20% Tripeptide			30% Tripeptide			40% Tripeptide			50% Tripeptide			60% Tripeptide			70% Tripeptide			80% Tripeptide			90% Tripeptide			100% Tripeptide		
	U	EV	NT	BL	U	EV	NT	BL	U	EV	NT	BL	U	EV	NT	BL	U	EV	NT	BL	U	EV	NT	BL	U	EV	NT	BL	U	EV	NT	BL	U	EV	NT	BL
0.3				7	3						6	4			4	6	1		2	7				10			1	9	1			1	8	3			7	3		7
0.25				3	4	3			3	3	4	5			3	7		1	2	7	1	2		7	1	3	6				10			1	9	3		7
0.2			8	2			5	5	6	3	3	3	1	9	1	2	3	1	2	6	1	4	5		1	1	8		3	1	6		2		8	1	2	1	6
0.15			10			10			9	1			10		8	1	1	8	1	1	9		1		8		2		5	5	1	5		4		6	1	3
0.1			10			10			10				10		10			10			9		1		10				10			10			3	7		

EV: elongated vesicle, NT: nanotube, BL: bilayer (lamellar) and U: unstructured/disordered. Color scheme is as follows: pink (vesicles/lamellae), purple (nanotubes/lamellae/vesicles), orange (nanotubes/lamellae), green (lamellar bilayers), and cyan (vesicles)

The phase space of the morphology of the nanostructures as a function of the total concentration of the peptides and the relative concentration of the tripeptides in Table 1 is further decomposed into four histograms, shown in Fig. 3–5 and ESI Fig. 1.† Each histogram summarizes the statistics for a given morphology of the hybrid nanostructure. Fig. 3 shows the frequency of occurrence of vesicles in the ten independent trajectories for every molecular composition examined in this study. The molecular composition constitutes the total concentration of peptides and the relative concentration of the tripeptides. Vesicles are consistently observed for the lower total concentrations of the peptides (0.1–0.15 peptides per nm^3).

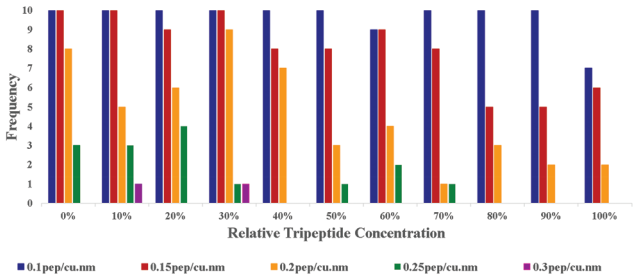

Fig. 3 Histogram of the occurrence of vesicles in mixtures of FF and FNF for different molecular compositions (that is, the values of the total peptide concentration and relative tripeptide concentration). These measurements used 10 independent particle trajectories for each molecular composition.

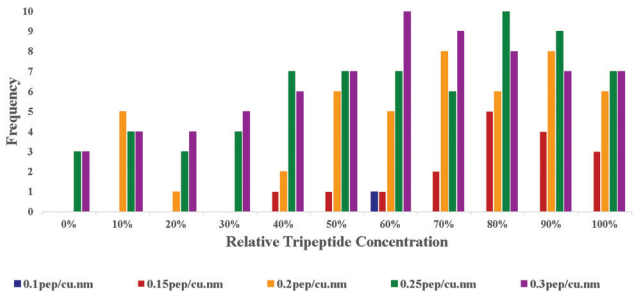

Fig. 4 Histogram of the occurrence of lamellar bilayers in mixtures of FF and FNF for different molecular compositions (that is, the values of the total peptide concentration and relative tripeptide concentration). These measurements used 10 independent particle trajectories for each molecular composition.

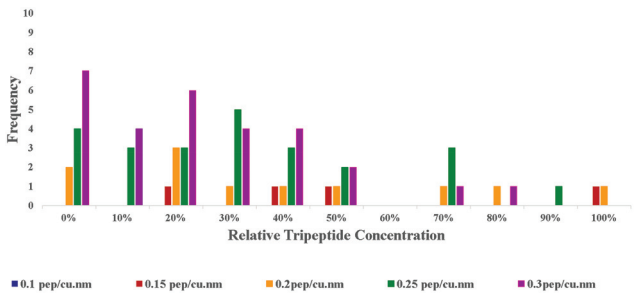

Fig. 5 Histogram of the occurrence of nanotubes in mixtures of FF and FNF for different molecular compositions (that is, the values of the total peptide concentration and relative tripeptide concentration). These measurements used 10 independent particle trajectories for each molecular composition.

As the total concentration of the peptides increases, the propensity of the peptides to form vesicles decreases. This trend is consistent across all relative tripeptide concentrations, ranging from 0% (a pure FF system) to 100% (a pure FNF system). Increasing the total concentration of peptides, however, increases the propensity of the peptides to form lamellar bilayers. This effect is particularly pronounced at 0.25 and 0.3 peptides per nm^3, as shown in Fig. 4. Lamellae are also observed at medium values of the total concentration of the peptides (0.2 peptides per nm^3) but only for high relative tripeptide concentrations (70%–100%).

Nanotubes are a relatively infrequent occurrence, but can be observed for higher values of the total concentration of peptides (0.2–0.3 peptides per nm^3) and low-to-medium relative tripeptide concentrations (20%–50%), as demonstrated in Fig. 5. Nanotubes are also observed when the net peptide concentrations are low and the relative tripeptide concentrations are high, for example, at 100% tripeptide with total concentrations of 0.1, 0.2, 0.25 and 0.3 peptides per nm^3. However, these are relatively rare occurrences.

The assembly pathways are observed to depend upon the relative concentration of tripeptides in the system. For FF alone, it has been shown experimentally and with exhaustive Monte Carlo simulations on discrete lattices that the peptide forms nanostructures in a concentration dependent fashion, from vesicles to nanotubes to lamellae.[73] We observe the same transitions using molecular dynamics at similar dipeptide concentrations, supporting the assumption that these calculations are approaching equilibrium. Similarly, Guo *et al.*[50] reported assembly pathways that included the fusion of smaller sized vesicles for pure FF systems with a low concentration of peptides and the folding of bilayers into nanotubes for a high concentration of peptides. This is thought to occur through a mechanism where, at low values of the total concentration of peptides (0.1–0.15 peptides per nm^3) (see Fig. 6), small vesicles are observed to diffuse in solution until they encounter other small vesicles and coalesce to form larger sized vesicles. At higher values of the relative tripeptide concentrations however, the peptides tend to assemble into a bilayer that then either stabilizes itself *via* periodic boundary interactions, or bends and closes its free edges to form a vesicle or a nanotube.

The morphology also depends on the relative concentrations of di- and tri-peptides. For all peptide ratios, we found a preference for vesicles at the lowest total peptide concentration, and lamellar bilayers at the highest total concentrations. In addition, we have identified an additional degree of freedom, *i.e.* the relative tripeptide concentration. From the statistics gathered from our simulations, we have constructed a molecular-composition phase-space diagram (presented in Fig. 7) that shows distinct molecular composition parameters promoting the formation of vesicles, lamellar bilayers and

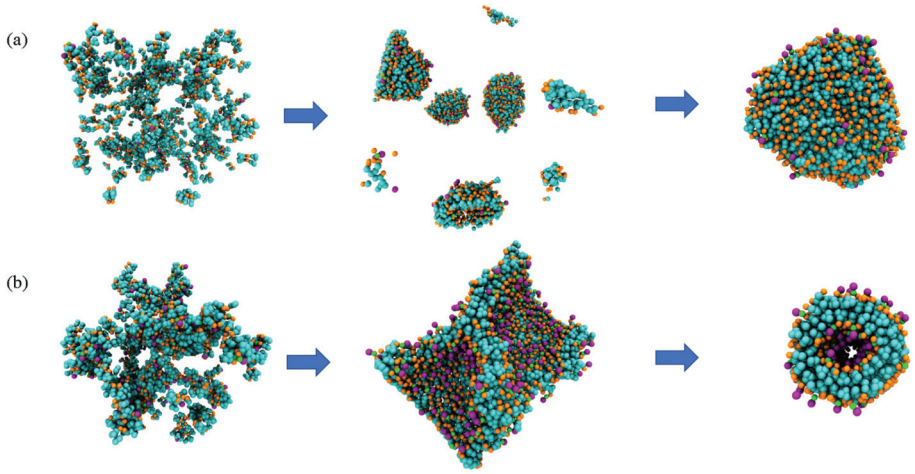

Fig. 6 Assembly pathways: (a) At low concentrations of both the total peptide as well as the relative tripeptide, smaller vesicles first form and then fuse into a larger vesicle. (b) At higher concentrations, bilayer like structures first form and then fuse their free edges into nanotubes or vesicles (nanotube shown here).

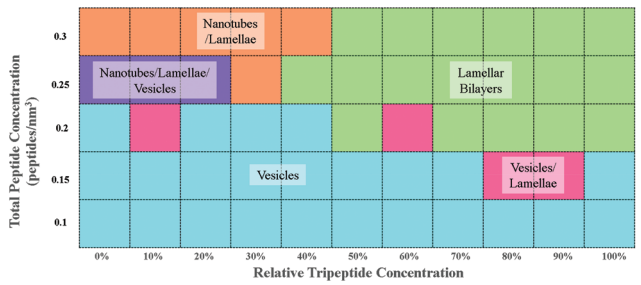

Fig. 7 Phase space map showing regimes of vesicles, nanotubes, and lamellar bilayers. Of the ten trajectories, the most representative structure is presented here. In the case where there are two or more structures listed, that is because they were close to equal representations of both morphologies.

nanotubes. At the bottom of the phase space (representing low total peptide concentrations), we find that the system is in the vesicle regime. We attribute this result to the fact that low total peptide concentrations do not form structures large enough to interact through periodic boundaries. Therefore, the most favorable configuration is a fully closed vesicle, as this morphology would minimize any interactions of the hydrophobic aromatic side chains with the water particles.

At higher total concentrations of peptides, as the size of the aggregates increase, the nanostructures in the systems have a higher tendency to interact through periodic walls and thereby, stabilizing themselves. The morphology of such nanostructures can be categorized by the number of period walls they interact through. Vesicles do not extend infinitely through periodic walls, nanotubes do so through two opposite periodic walls, and lamellar bilayers, through four periodic walls. To the upper left portion of the molecular composition phase space (shown in Fig. 7), there is an overlap between the nanotube and bilayer regimes. This regime overlap is attributed to two competing effects: the tendency of the peptides to form bilayers at high concentrations, and the curvature-inducing effect of the tripeptides in low-to-medium relative tripeptide concentrations.

Fig. 8 shows the competing forces acting on a FNF tripeptide molecule that is embedded in a bilayer. The competing forces include the electrostatic attraction between adjacent C and N termini of the peptides, favorable hydrophilic interactions between the backbones and the asparagine side chain and the solvent particles, and favorable hydrophobic interactions between the aromatic phenylalanine side chains. These various forces create a force differential, which coupled to the hinge-like structure of the tripeptide, due to the presence of asparagine in the middle, makes this force differential manifest as a "pinching" effect that induces curvature. To quantify this effect, the average angle made by the FNF backbone was measured (see Fig. 9).

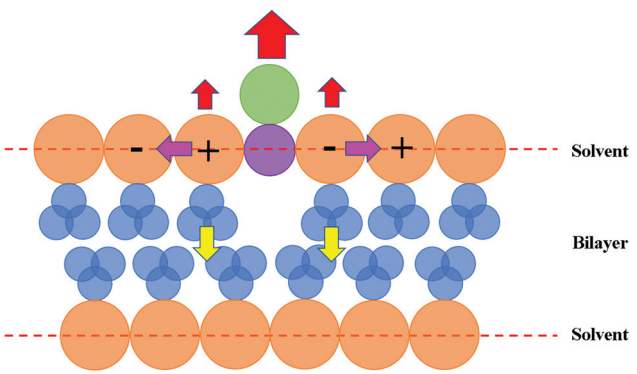

Fig. 8 Tripeptide in a bilayer: yellow arrows represent the hydrophobic attraction between aromatic side chains. Red arrows represent hydrophilic interactions between amino acid backbones and the asparagine side chains and water particles. Purple arrows indicate the electrostatic attraction between the C and N termini. The resultant force differential tends to induce curvature in a FF-FNF bilayer.

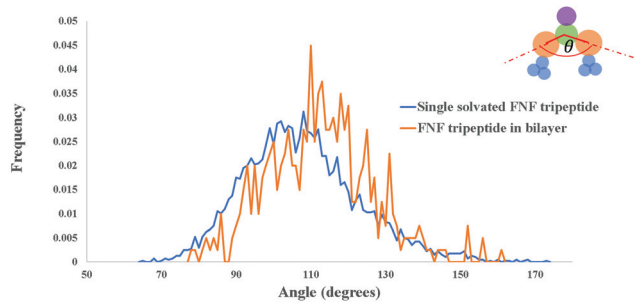

Fig. 9 Distribution of the angle (theta) of the tripeptide (FNF). The average angle is 112.9°, compared to the equilibrium angle of a single solvated FNF peptide pf 107.4°.

The angle between the backbone beads (~113°) is significantly distorted as compared to the equilibrium angle (107°). This indicates that the tripeptide stretches laterally while the asparagine side chain experiences an attractive force, pulling it into the solvent and keeping the hinge correctly aligned, thereby inducing a local curvature in the bilayer.

To the upper right of the phase map (see Fig. 7), the lamellar bilayers are observed to dominate the molecular composition phase space. We attribute this result to the fact that in addition to the high overall peptide concentration, the high tripeptide concentration makes it far more likely that the tripeptides are distributed uniformly on either side of the bilayer. This uniform distribution negates any preference to induce local curvature in a specific direction. A representative example of the bilayer tripeptide spatial distribution is measured and shown in Fig. 10. At lower tripeptide concentrations, a difference can be observed in the distribution of peptides on either side of the bilayer for different morphologies. This is demonstrated in Table 2.

At high relative tripeptide concentrations (90%–100%), a small number of irregular or disordered nanostructures are observed (see Fig. 11). This suggests that an overabundance of tripeptide "hinges" in the bilayer decreases its ability to attain

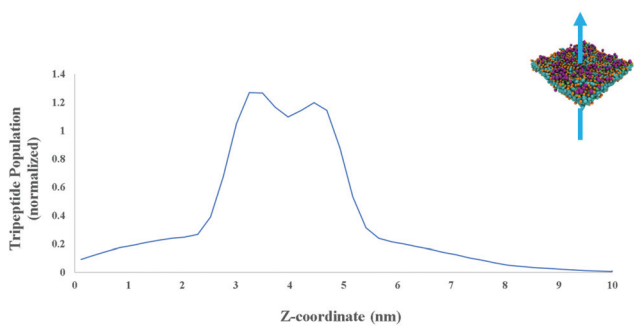

Fig. 10 Population density of FNF tripeptides plotted against the Z axis coordinate for total peptide concentration = 0.3 peptides per nm^3 and relative tripeptide concentration of 50%. Two closely spaced peaks show that the tripeptide distributes itself relatively evenly on both sides of the bilayer, leading to the lamella lacking a preference to fold in any specific direction.

Table 2 Distribution of tripeptides on either side of the bilayer for different morphologies. The total peptide concentration is 0.25 peptides per nm^3 at 10% tripeptide concentration. A representative system for each morphology was chosen and the number of peptides on either side of the bilayer were counted

	Nanotube	Vesicle	Lamella
Inside	13	19	24 (top)
Outside	37	31	26 (bottom)

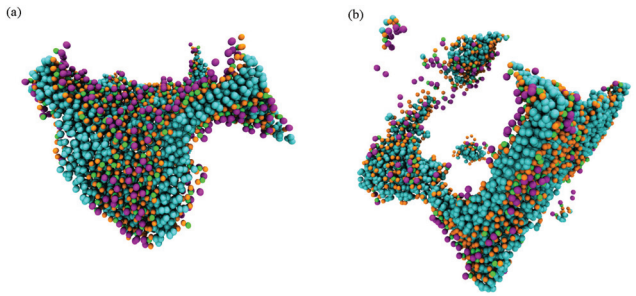

Fig. 11 Disordered assembly occurring at 0.3 peptides per nm^3 and (a) 90% tripeptide, (b) 50% tripeptide.

a stable morphology. Additionally, overlaps are observed in the domains of the three main morphologies (that is, vesicles, nanotubes and lamellae). This indicates a transition between morphologies for specific values of the total concentration of peptides and relative concentrations of the tripeptides. It is important to note that nanotubes do not have an exclusive molecular composition parameter space like lamellae or vesicles.

Conclusions

We explored the impact of molecular composition on the morphology of phenylalanine-based hybrid biological materials. We focused our investigation on peptide species with different polar groups but identical hydrophobic groups, that is FF and FNF. We examined the morphology of the self-assembled hybrid, peptide nanostructures by varying the molecular composition. The molecular composition constituted five total concentrations of the peptides and eleven relative concentrations of the tripeptides (FNF). We used MD simulation in conjunction with CG models to study the large molecular composition parameter space.

Our results demonstrate a rich polymorphism in the assembly of these peptide mixtures. Distinct molecular composition regimes promoting the formation of vesicles, nanotubes and lamellar bilayers have been identified. The morphology of self-assembled nanostructures is observed to depend upon both the total concentration of peptides as well as the relative tripeptide concentration. Low concentrations (~20–30%) of FNF tripeptides, when mixed with FF dipeptides, while maintaining a very high total peptide concentration (~0.3 peptides per

nm^3), display the greatest diversity of the assembled structures. This region of the molecular composition parameter space yields vesicles, nanotubes and lamellar bilayers. We propose that this finding arises due to the competing effects of the high total concentration of peptides biasing the system towards lamellar bilayers and the presence of the tripeptides inducing local curvature in the self-assembled hybrid nanostructures. This unique behavior is attributed to the molecular structure of the FNF tripeptide.

The results from this investigation demonstrate that the morphology of the phenylalanine-based hybrid biological materials is controlled *via* the molecular composition. Our findings can be used to potentially guide the selection of peptides for the design of novel hybrid biological materials with target morphologies: specifically, sequences of peptides with carefully placed hydrophobic and hydrophilic regions and charges can be selected to design novel peptide sequences that assemble into nanostructures with target morphologies and other characteristics.

Conflicts of interest

There are no conflicts to declare.

Acknowledgements

The authors gratefully acknowledge computational resources provided by the eXtreme Science and Engineering Discovery Environment (XSEDE) allocation TG-DMR140125, and the San Diego Supercomputing Center (SDSC). The authors would like to thank Daniel Grisham and Tianyou Mou for insightful discussions on the study. SM acknowledges the Molecular Sciences Software Institute (MolSSI) for their support. KS would like to thank and acknowledge the New Jersey Space Grant Consortium for their support. MD gratefully acknowledges financial support from NSF CAREER-1654325.

References

1 K. E. Marshall, D. M. Vadukul, L. Dahal, A. Theisen, M. W. Fowler, Y. Al-Hilaly, L. Ford, G. Kemenes, I. J. Day, K. Staras and L. C. Serpell, A critical role for the self-assembly of Amyloid-beta 1–42 in neurodegeneration, *Sci. Rep.*, 2016, **6**, 30182.

2 Z. S. Al-Garawi, K. L. Morris, K. E. Marshall, J. Eichler and L. C. Serpell, The diversity and utility of amyloid fibrils formed by short amyloidogenic peptides, *Interface Focus*, 2017, **7**(6), 20170027.

3 L. Deng and H. Xu, Hierarchical processes in beta-sheet peptide self-assembly from the microscopic to the mesoscopic level, *Chin. Phys. B*, 2016, **25**(1), 018701.

4 T. D. Do, N. E. C. de Almeida, N. E. LaPointe, A. Chamas, S. C. Feinstein and M. T. Bowers, Amino Acid Metaclusters: Implications of Growth Trends on Peptide Self-Assembly and Structure, *Anal. Chem.*, 2016, **88**(1), 868–876.

5 P. C. Ke, M. A. Sani, F. Ding, A. Kakinen, I. Javed, F. Separovic, T. P. Davis and R. Mezzenga, Implications of peptide assemblies in amyloid diseases, *Chem. Soc. Rev.*, 2017, **46**(21), 6492–6531.

6 M. Waqas, W. J. Jeong, Y. J. Lee, D. H. Kim, C. Ryou and Y. B. Lim, pH-Dependent In-Cell Self-Assembly of Peptide Inhibitors Increases the Anti-Prion Activity While Decreasing the Cytotoxicity, *Biomacromolecules*, 2017, **18**(3), 943–950.

7 J. Chen, B. Zhang, F. Xia, Y. C. Xie, S. F. Jiang, R. Su, Y. Lu and W. Wu, Transmembrane delivery of anticancer drugs through self-assembly of cyclic peptide nanotubes, *Nanoscale*, 2016, **8**(13), 7127–7136.

8 J. A. Hutchinson, S. Burholt and I. W. Hamley, Peptide hormones and lipopeptides: from self-assembly to therapeutic applications, *J. Pept. Sci.*, 2017, **23**(2), 82–94.

9 M. T. Jeena, L. Palanikumar, E. M. Go, I. Kim, M. G. Kang, S. Lee, S. Park, H. Choi, C. Kim, S. M. Jin, S. C. Bae, H. W. Rhee, E. Lee, S. K. Kwak and J. H. Ryu, Mitochondria localization induced self-assembly of peptide amphiphiles for cellular dysfunction, *Nat. Commun.*, 2017, **8**, 27.

10 B. H. San, Y. Li, E. B. Tarbet and S. M. Yu, Nanoparticle Assembly and Gelatin Binding Mediated by Triple Helical Collagen Mimetic Peptide, *ACS Appl. Mater. Interfaces*, 2016, **8**(31), 19907–19915.

11 T. Zohrabi and N. Habibi, Dendritic Peptide Nanostructures Formed from Self-Assembly of Di-L-phenylalanine Extracted from Alzheimer's beta-Amyloid Poly Peptides: Insights into Their Assembly Process, *Int. J. Pept. Res. Ther.*, 2015, **21**(4), 423–431.

12 J. Fan, L. Liu, S. M. Ding, M. L. Fu, F. F. Liu, C. C. Zhang, H. Wu, J. H. Wang and Y. Q. Qin, Studies on polymer capped quantum dots and peptide self-assembly using fluorescence coupled capillary electrophoresis, *Int. Nanoelectron. Conf.*, 2016, 1–2.

13 J. M. Lim, M. Y. Ryu, J. W. Yun, T. J. Park and J. P. Park, Electrochemical peptide sensor for diagnosing adenoma-carcinoma transition in colon cancer, *Biosens. Bioelectron.*, 2017, **98**, 330–337.

14 R. A. Mansbach and A. L. Ferguson, Coarse-Grained Molecular Simulation of the Hierarchical Self-Assembly of pi-Conjugated Optoelectronic Peptides, *J. Phys. Chem. B*, 2017, **121**(7), 1684–1706.

15 V. Nguyen, R. Zhu, K. Jenkins and R. S. Yang, Self-assembly of diphenylalanine peptide with controlled polarization for power generation, *Nat. Commun.*, 2016, **7**, 13566.

16 B. Adibi-Motlagh, A. S. Lotfi, A. Rezaei and E. Hashemi, Cell attachment evaluation of the immobilized bioactive peptide on a nanographene oxide composite, *Mater. Sci. Eng., C*, 2018, **82**, 323–329.

17 J. Banerjee and H. S. Azevedo, Crafting of functional biomaterials by directed molecular self-assembly of triple helical peptide building blocks, *Interface Focus*, 2017, **7**(6), 20160138.

18 E. Bartolami, J. Knoops, Y. Bessin, M. Fossepre, J. Chamieh, P. Dumy, M. Surin and S. Ulrich, One-Pot Self-Assembly of Peptide-Based Cage-Type Nanostructures Using Orthogonal Ligations, *Chem. – Eur. J.*, 2017, **23**(57), 14323–14331.

19 S. Basak, I. Singh, A. Ferranco, J. Syed and H. B. Kraatz, On the Role of Chirality in Guiding the Self-Assembly of Peptides, *Angew. Chem., Int. Ed.*, 2017, **56**(43), 13288–13292.

20 V. Castelletto, A. Kaur, I. W. Hamley, R. H. Barnes, K. A. Karatzas, D. Hermida-Merino, S. Swioklo, C. J. Connon, J. Stasiak, M. Reza and J. Ruokolainen, Hybrid membrane biomaterials from self-assembly in polysaccharide and peptide amphiphile mixtures: controllable structural and mechanical properties and antimicrobial activity, *RSC Adv.*, 2017, **7**(14), 8366–8375.

21 C. Chang, P. Q. Liang, L. L. Chen, J. F. Liu, S. H. Chen, G. H. Zheng and C. Y. Quan, pH-responsive nanoparticle assembly from peptide amphiphiles for tumor targeting drug delivery, *J. Biomater. Sci., Polym. Ed.*, 2017, **28**(13), 1338–1350.

22 F. Clerici, E. Erba, M. L. Gelmi and S. Pellegrino, Non-standard amino acids and peptides: From self-assembly to nanomaterials, *Tetrahedron Lett.*, 2016, **57**(50), 5540–5550.

23 A. Dasgupta, Exploring architectures at the nanoscale: the interplay between hydrophobic twin lipid chains and head groups of designer peptide amphiphiles in the self-assembly process and application, *Soft Matter*, 2016, **12**(19), 4352–4360.

24 M. C. Hsieh, D. G. Lynn and M. A. Grover, Kinetic Model for Two-Step Nucleation of Peptide Assembly, *J. Phys. Chem. B*, 2017, **121**(31), 7401–7411.

25 H. Y. Han, P. H. Weinreb and P. T. Lansbury, The Core Alzheimers Peptide Nac Forms Amyloid Fibrils Which Seed and Are Seeded by Beta-Amyloid - Is Nac a Common Trigger or Target in Neurodegenerative Disease, *Chem. Biol.*, 1995, **2**(3), 163–169.

26 E. Gazit, Mechanistic studies of the process of amyloid fibrils formation by the use of peptide fragments and, analogues: Implications for the design of fibrillization inhibitors, *Curr. Med. Chem.*, 2002, **9**(19), 1725–1735.

27 D. Zanuy, Y. Porat, E. Gazit and R. Nussinov, Peptide sequence and amyloid formation: Molecular simulations and experimental study of a human islet amyloid polypeptide fragment and its analogs, *Structure*, 2004, **12**(3), 439–455.

28 M. Reches and E. Gazit, Self-assembly of peptide nanotubes and amyloid-like structures by charged-termini-capped diphenylalanine peptide analogues, *Isr. J. Chem.*, 2005, **45**(3), 363–371.

29 S. Gilead and E. Gazit, Self-organization of short peptide fragments: From amyloid fibrils to nanoscale supramolecular assemblies, *Supramol. Chem.*, 2005, **17**(1–2), 87–92.

30 M. Reches and E. Gazit, Casting metal nanowires within discrete self-assembled peptide nanotubes, *Science*, 2003, **300**(5619), 625–627.

31 M. Yemini, M. Reches, E. Gazit and J. Rishpon, Peptide nanotube-modified electrodes for enzyme-biosensor applications, *Anal. Chem.*, 2005, **77**(16), 5155–5159.

32 M. Reches and E. Gazit, Self-assembly of peptide nanotubes and amyloid-like structures by charged-termini capped diphenylalanine peptide analogues, *FEBS J.*, 2005, **272**, 388–388.

33 N. Kol, L. Adler-Abramovich, D. Barlam, R. Z. Shneck, E. Gazit and I. Rousso, Self-assembled peptide nanotubes are uniquely rigid bioinspired supramolecular structures, *Nano Lett.*, 2005, **5**(7), 1343–1346.

34 E. Gazit and M. Reches, Self-assembly of peptide nanotubes by charged-termini capped diphenylalanine peptide analogue, *Abstr. Pap. Am. Chem. Soc.*, 2005, **229**, U1154–U1154.

35 M. Reches and E. Gazit, Controlled patterning of aligned self-assembled peptide nanotubes, *Nat. Nanotechnol.*, 2006, **1**(3), 195–200.

36 O. Carny, D. E. Shalev and E. Gazit, Fabrication of coaxial metal nanocables using a self-assembled peptide nanotube scaffold, *Nano Lett.*, 2006, **6**(8), 1594–1597.

37 M. Reches and E. Gazit, Molecular self-assembly of peptide nanostructures: mechanism of association and potential uses, *Curr. Nanosci.*, 2006, **2**(2), 105–111.

38 E. Gazit, A. Boman, H. G. Boman and Y. Shai, Interaction of the Mammalian Antibacterial Peptide Cecropin P1 with Phospholipid-Vesicles, *Biochemistry*, 1995, **34**(36), 11479–11488.

39 S. Ghosh, M. Reches, E. Gazit and S. Verma, Bioinspired design of nanocages by self-assembling triskelion peptide elements, *Angew. Chem., Int. Ed.*, 2007, **46**(12), 2002–2004.

40 K. Kornmueller, B. Lehofer, C. Meindl, E. Frohlich, G. Leitinger, H. Amenitsch and R. Prassl, Peptides at the Interface: Self-Assembly of Amphiphilic Designer Peptides and Their Membrane Interaction Propensity, *Biomacromolecules*, 2016, **17**(11), 3591–3601.

41 I. W. Hamley, J. Hutchinson, S. Kirkham, V. Castelletto, A. Kaur, M. Reza and J. Ruokolainen, Nanosheet Formation by an Anionic Surfactant-like Peptide and Modulation of Self-Assembly through Ionic Complexation, *Langmuir*, 2016, **32**(40), 10387–10393.

42 S. G. Zhang, Discovery and design of self-assembling peptides, *Interface Focus*, 2017, **7**(6), 20170028.

43 E. L. Magnotti, S. A. Hughes, R. S. Dillard, S. Y. Wang, L. Hough, A. Karumbamkandathil, T. Q. Lian, J. S. Wall, X. B. Zuo, E. R. Wright and V. P. Conticello, Self-Assembly of an alpha-Helical Peptide into a Crystalline Two-Dimensional Nanoporous Framework, *J. Am. Chem. Soc.*, 2016, **138**(50), 16274–16282.

44 L. Adler-Abramovich and E. Gazit, Controlled patterning of peptide nanotubes and nanospheres using inkjet printing technology, *J. Pept. Sci.*, 2008, **14**(2), 217–223.

45 M. Reches and E. Gazit, Biological and chemical decoration of peptide nanostructures via biotin-avidin interactions, *J. Nanosci. Nanotechnol.*, 2007, **7**(7), 2239–2245.

46 E. Gazit, Self-assembled peptide nanostructures: the design of molecular building blocks and their technological utilization, *Chem. Soc. Rev.*, 2007, **36**(8), 1263–1269.
47 M. J. Krysmann, V. Castelletto, J. E. McKendrick, L. A. Clifton, I. W. Hamley, P. J. F. Harris and S. A. King, Self-assembly of peptide nanotubes in an organic solvent, *Langmuir*, 2008, **24**(15), 8158–8162.
48 P. W. J. M. Frederix, R. V. Ulijn, N. T. Hunt and T. Tuttle, Virtual Screening for Dipeptide Aggregation: Toward Predictive Tools for Peptide Self-Assembly, *J. Phys. Chem. Lett.*, 2011, **2**(19), 2380–2384.
49 R. L. Huang, R. X. Su, W. Qi, J. Zhao and Z. M. He, Hierarchical, interface-induced self-assembly of diphenylalanine: formation of peptide nanofibers and microvesicles, *Nanotechnology*, 2011, **22**(24), 245609.
50 C. Guo, Y. Luo, R. H. Zhou and G. H. Wei, Probing the Self-Assembly Mechanism of Diphenylalanine-Based Peptide Nanovesicles and Nanotubes, *ACS Nano*, 2012, **6**(5), 3907–3918.
51 A. N. Rissanou, E. Georgilis, E. Kasotaids, A. Mitraki and V. Harmandaris, Effect of Solvent on the Self-Assembly of Dialanine and Diphenylalanine Peptides, *J. Phys. Chem. B*, 2013, **117**(15), 3962–3975.
52 Y. Q. Lu, M. F. Wang, W. Qi, R. X. Su and Z. M. He, Artificial Hydrolase Based on Short Peptides Self- and Co-assembly Nanofiber, *Chem. J. Chin. Univ.*, 2015, **36**(7), 1304–1309.
53 L. Adler-Abramovich, P. Marco, Z. A. Amon, R. C. G. Creasey, T. C. T. Michaels, A. Levin, D. J. Scurr, C. J. Roberts, T. P. J. Knowles, S. J. B. Tendler and E. Gazit, Controlling the Physical Dimensions of Peptide Nanotubes by Supramolecular Polymer Coassembly, *ACS Nano*, 2016, **10**(8), 7436–7442.
54 C. Guo, Z. A. Amon, R. X. Qi, Q. W. Zhang, L. Adler-Abramovich, E. Gazit and G. H. Wei, Expanding the Nanoarchitectural Diversity Through Aromatic Di- and Tri-Peptide Coassembly: Nanostructures and Molecular Mechanisms, *ACS Nano*, 2016, **10**(9), 8316–8324.
55 S. J. Marrink, H. J. Risselada, S. Yefimov, D. P. Tieleman and A. H. de Vries, The MARTINI force field: Coarse grained model for biomolecular simulations, *J. Phys. Chem. B*, 2007, **111**(27), 7812–7824.
56 L. Monticelli, S. K. Kandasamy, X. Periole, R. G. Larson, D. P. Tieleman and S. J. Marrink, The MARTINI coarse-grained force field: Extension to proteins, *J. Chem. Theory Comput.*, 2008, **4**(5), 819–834.
57 D. H. de Jong, G. Singh, W. F. D. Bennett, C. Arnarez, T. A. Wassenaar, L. V. Schafer, X. Periole, D. P. Tieleman and S. J. Marrink, Improved Parameters for the Martini Coarse-Grained Protein Force Field, *J. Chem. Theory Comput.*, 2013, **9**(1), 687–697.
58 H. Bekker, H. J. C. Berendsen, E. J. Dijkstra, S. Achterop, R. Vondrumen, D. Vanderspoel, A. Sijbers, H. Keegstra, B. Reitsma and M. K. R. Renardus, Gromacs - a Parallel Computer for Molecular-Dynamics Simulations, *Physics Computing '92*, 1993, 252–256.
59 H. J. C. Berendsen, D. Vanderspoel and R. Vandrunen, Gromacs - a Message-Passing Parallel Molecular-Dynamics Implementation, *Comput. Phys. Commun.*, 1995, **91**(1–3), 43–56.
60 R. Vandrunen, D. Vanderspoel and H. J. C. Berendsen, Gromacs - a Software Package and a Parallel Computer for Molecular-Dynamics, *Abstr. Pap. Am. Chem. Soc.*, 1995, **209**, 49-Comp.
61 D. Van der Spoel, E. Lindahl, B. Hess, G. Groenhof, A. E. Mark and H. J. C. Berendsen, GROMACS: Fast, flexible, and free, *J. Comput. Chem.*, 2005, **26**(16), 1701–1718.
62 N. Goga, I. Marin, A. Vasilateanu, I. B. Pavaloiu, K. O. Kadiri and O. Awodele, Improved GROMACS Algorithms using the MPI Parallelization, *2015 E-Health and Bioengineering Conference (Ehb)*, 2015.
63 G. Bussi, D. Donadio and M. Parrinello, Canonical sampling through velocity rescaling, *J. Chem. Phys.*, 2007, **126**(1), 014101.
64 G. Bussi, T. Zykova-Timan and M. Parrinello, Isothermal-isobaric molecular dynamics using stochastic velocity rescaling, *J. Chem. Phys.*, 2009, **130**(7), 074101.
65 M. Parrinello and A. Rahman, Crystal-Structure and Pair Potentials - a Molecular-Dynamics Study, *Phys. Rev. Lett.*, 1980, **45**(14), 1196–1199.
66 M. Parrinello and A. Rahman, A Molecular-Dynamics Study of Crystal-Structure Transformations, *Bull. Am. Phys. Soc.*, 1981, **26**(3), 380–380.
67 M. Parrinello and A. Rahman, Polymorphic Transitions in Single-Crystals - a New Molecular-Dynamics Method, *J. Appl. Phys.*, 1981, **52**(12), 7182–7190.
68 F. Aydin, P. Ludford and M. Dutt, Phase segregation in bio-inspired multi-component vesicles encompassing double tail phospholipid species, *Soft Matter*, 2014, **10**(32), 6096–6108.
69 F. Aydin, G. Uppaladadium and M. Dutt, Harnessing Nanoscale Confinement to Design Sterically Stable Vesicles of Specific Shapes via Self-Assembly, *J. Phys. Chem. B*, 2015, **119**(32), 10207–10215.
70 F. Aydin, G. Uppaladadium and M. Dutt, The design of shape-tunable hairy vesicles, *Colloids Surf., B*, 2015, **128**, 268–275.
71 S. A. Walker, S. Chiruvolu, J. A. Zasadzinski, F. J. Schmitt and J. N. Israelachvili, Controlled multi-stage self-assembly of vesicles, in *Hollow and Solid Spheres and Microspheres: Science and Technology Associated with Their Fabrication and Application*, 1995, vol. 372, pp. 95–100.
72 J. N. Israelachvili, *Thermodynamic Principles of Self-Assembly. Intermolecular and Surface Forces*, 3rd edn, 2011, pp. 503–534.
73 Y. J. Song, S. R. Challa, C. J. Medforth, Y. Qiu, R. K. Watt, D. Pena, J. E. Miller, F. van Swol and J. A. Shelnutt, Synthesis of peptide-nanotube platinum-nanoparticle composites, *Chem. Commun.*, 2004, (9), 1044–1045.